

1 Novel techniques to search for neutron radioactivity

2 M. Thoennessen^{a,b,*}, G. Christian^c, Z. Kohley^{a,d}, T. Baumann^a, M. Jones^{a,b},
3 J. K. Smith^{a,b}, J. Snyder^{a,b}, A. Spyrou^{a,b}

4 ^a*National Superconducting Cyclotron Laboratory, Michigan State University, East Lansing,*
5 *Michigan 48824*

6 ^b*Department of Physics & Astronomy, Michigan State University, East Lansing, Michigan*
7 *48824*

8 ^c*TRIUMF, 4004 Wesbrook Mall, Vancouver, British Columbia V6T 2A3, Canada*

9 ^d*Department of Chemistry, Michigan State University, East Lansing, Michigan 48824*

10 Abstract

11 Two new methods to observe neutron radioactivity are presented. Both
12 methods rely on the production and decay of the parent nucleus in flight. The
13 relative velocity measured between the neutron and the fragment is sensitive
14 to half-lives between ~ 1 and ~ 100 ps for the Decay in Target (DiT) method.
15 The transverse position measurement of the neutron in the Decay in a Magnetic
16 Field (DiMF) method is sensitive to half-lives between 10 ps and 1 ns.

17 *Keywords:* Neutron spectroscopy, Neutron radioactivity

18 1. Introduction

19 Nuclei with extreme neutron deficiency or neutron excess can decay by the
20 emission of one or more protons or neutrons, respectively. The presence of the
21 Coulomb barrier can significantly hinder the emission of a proton which can
22 lead to fairly long lifetimes for this decay mode. The current status of one- and
23 two-proton radioactivity has recently been reviewed by Pfützner [1]. In con-
24 trast, neutron emission typically proceeds on very short time scales ($\sim 10^{-21}$ s),
25 primarily due to the absence of the Coulomb barrier. However, it has been
26 postulated that in special cases one- or two-neutron radioactivity might occur
27 due to the presence of an angular momentum barrier [2–4]. Lifetimes as short
28 as 10^{-12} s can be considered as radioactivity [5] and only in the most extreme
29 cases neutron emission is expected to reach these time scales. Thus traditional

*Corresponding Author.
Preprint submitted to Nucl. Instrum. Meth. A
Email address: thoennessen@nscl.msu.edu (M. Thoennessen)

30 methods where the decaying nucleus is implanted in a detector and the subse-
31 quent decay is recorded are not applicable. With these methods the shortest
32 measured lifetimes at present are 620 ns [6, 7] and 1.9 μ s [8–10] for α - and
33 proton-decay, respectively.

34 Mukha *et al.* developed a new technique to measure the two-proton decay
35 of ^{19}Mg in flight by tracking the paths of the decay products and measured a
36 half-life of 4.0(15) ps [11]. Voss *et al.* studied the same decay with an adapta-
37 tion of the recoil distance method. The degrader foil of a plunger device was
38 replaced by a double-sided silicon strip detector to measure the energy-loss of
39 the decaying nucleus (^{19}Mg) and the resulting fragment (^{17}Ne). The lifetime
40 was then extracted from the intensity ratio of the energy loss peaks as a function
41 of target to detector distance [12].

42 In order to search for the corresponding decays of neutron-rich nuclei these
43 or similar techniques have to be developed for neutron emission. Grigorenko *et*
44 *al.* suggested one might adapt the tracking method by measuring the angular
45 distributions of the neutron(s) and the fragment with high precision [3]. The
46 reconstructed opening angle of the decay is then directly related to the decay
47 energy. Caesar *et al.* extracted an upper limit of 5.7 ns for the decay of ^{26}O
48 by two-neutron emission by assuming the survival of ^{26}O along the flight path
49 in a magnetic field [13]. For future experiments they also proposed placing
50 the target directly in front of a deflecting magnet and then deducing the life-
51 time from the horizontal position distribution of the neutrons. Most recently
52 Kohley *et al.* applied another modification of the recoil distance method to
53 analyze the previously reported ground-state two-neutron decay of ^{26}O [14]. In
54 this method the velocity difference between the neutrons and the fragments is
55 sensitive to the lifetime if the decay occurs within the target. A half-life of
56 $4.5_{-1.5}^{+1.1}(\text{stat}) \pm 3(\text{syst})$ ps was determined for the decay of ^{26}O [15].

57 In the present paper we discuss calculations to extract the half-life sensitivi-
58 ties of the two methods mentioned above: the velocity difference method for the
59 Decay in the Target (DiT) and the method to measure the horizontal neutron
60 position distribution following the Decay in a Magnetic Field (DiMF).

61 **2. Test case of ^{16}B**

62 In order to explore the feasibility of the DiT and DiMF methods for the
63 measurement of neutron radioactivity, the single neutron decay of ^{16}B was used
64 as a test case. Although it is unlikely that neutron radioactivity will be observed
65 in ^{16}B , the reaction $^{17}\text{C}(-\text{p})^{16}\text{B} \rightarrow ^{15}\text{B} + \text{n}$ was simulated because the compli-
66 cations due to the emission of multiple neutrons, occurring in the potentially
67 more interesting case of the two-neutron emitter ^{26}O , are avoided.

68 ^{16}B is unbound with respect to ^{15}B plus a neutron [16, 17] and the ground
69 state resonance was reported at 40(60) keV [19] and 40(40) keV [18] from mul-
70 tiparticle transfer reactions. Such a low decay energy (which is consistent with
71 0 keV within the given uncertainty) is critical for the possible observation of
72 a finite lifetime because of the small barrier which is only due to the angular
73 momentum. For an $l=2$ transition, which is expected for the ground state of
74 ^{16}B , a decay energy of about 1 keV corresponds to a half-life of approximately
75 0.1 ps [2, 4]. Subsequently, invariant mass measurements found a resonance at
76 low decay energies of 85(15) keV [20] and 60(20) keV [21]. This resonance most
77 likely corresponds to the ground state decay. However, it is still conceivable
78 that it could be a transition to one of the bound excited states of ^{15}B . In an
79 attempt to search for neutron radioactivity of ^{16}B an upper limit for the half-life
80 of 132 ps (68% confidence level) was extracted from a proton stripping reaction
81 from a radioactive ^{17}C beam [2].

82 **3. Decay in Target (DiT)**

83 The DiT technique was recently applied for the first time in the decay of
84 ^{26}O into ^{24}O and two neutrons [15]. A schematic overview of this technique is
85 shown in figure 1 for the decay of ^{16}B as an example. In this figure it is assumed
86 that the one-proton removal reaction $^{17}\text{C}(-\text{p})^{16}\text{B}$ occurs at the beginning of the
87 target and the outgoing fragment continues with essentially the same velocity
88 as the incoming beam. As mentioned before, in order for long lifetimes to occur
89 the decay energy for the subsequent decay of ^{16}B into ^{15}B and a neutron has

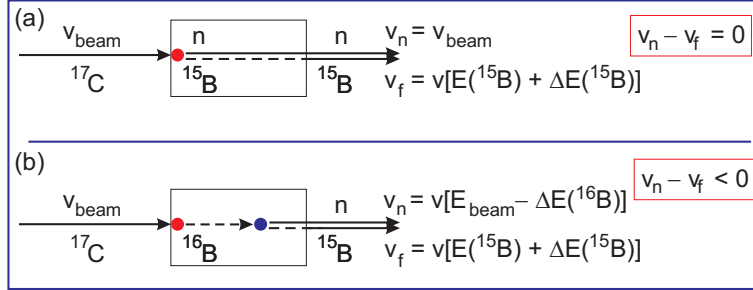


Figure 1: Schematics of the DiT technique. Panel (a) shows the production of ^{16}B and decay to ^{15}B at the beginning of the target, while in panel (b) ^{16}B is produced at the beginning of the target but decays to ^{15}B and a neutron at a later time in the target. Because the position of the decay is unknown, $\Delta E(^{15}\text{B})$ is calculated assuming it traverses the whole target. The calculations of the relevant velocities are explained in the text.

90 to be very low and therefore recoil effects can be neglected. Panel (a) of the
 91 figure depicts the situation where the decay of ^{16}B into ^{15}B and a neutron pro-
 92 ceeds instantaneously. While the neutrons continue at beam velocity through
 93 the target and into the neutron detectors, the ^{15}B fragments lose energy as they
 94 traverse the target before the final energy is measured with charged-particle
 95 detectors. The fragment velocity at the interaction point can then be recon-
 96 structed from the measured final energy $[E(^{15}\text{B})]$ and the energy loss through
 97 the target $[\Delta E(^{15}\text{B})]$ which can be calculated with the above assumptions from
 98 the incoming beam energy and the target thickness. The velocity difference $v_n -$
 99 v_f for this case is then equal to zero. If the decay occurs at a later time, when
 100 the ^{16}B fragment has traveled through a fraction of the target, the calculated
 101 velocity difference will be less than zero as shown in figure 1(b). As the location
 102 of the decay is unknown, the fragment velocity is calculated with the assump-
 103 tion that the decay occurred at the beginning of the target, the same as in panel
 104 (a). The neutron velocity, however, will be reduced due to the energy loss of
 105 the ^{16}B in the target before its decay to ^{15}B and the neutron. The signature
 106 for a finite lifetime of the decay is thus a shift towards negative values of the
 107 velocity difference $v_n - v_f$.

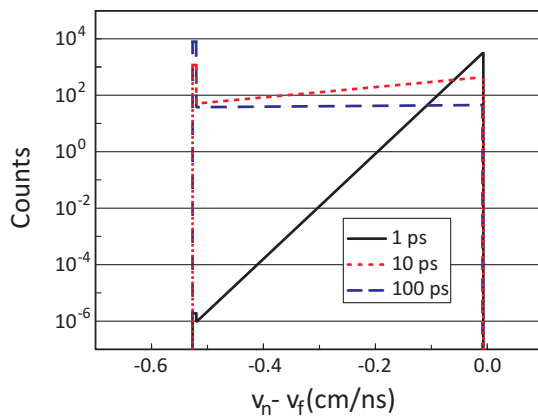


Figure 2: Velocity difference distributions for the decay of ^{16}B into ^{15}B and a neutron at 80 MeV/u for three different half lives. The production of ^{16}B is assumed to occur at the beginning of a 700 mg/cm^2 ^9Be target. The fragment velocity was calculated after adding the energy loss of the fragment through the whole target to the final measured energy.

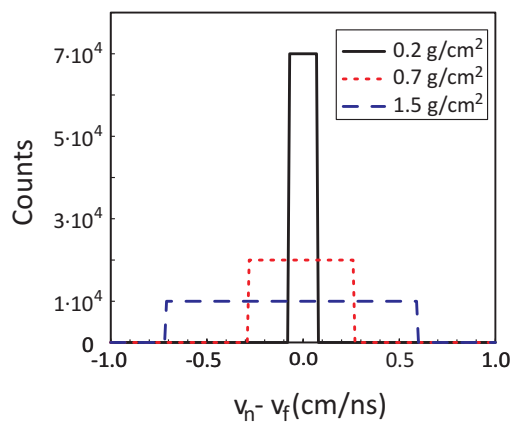


Figure 3: Velocity difference distributions from the instantaneous decay of ^{16}B ($t_{1/2} = 0 \text{ ps}$) to ^{15}B for three different target thicknesses at an incident beam energy of 80 MeV/u. For these curves it was assumed that ^{16}B could be produced (and decay instantaneously) anywhere equally distributed throughout the target. The energy loss of the fragments through only half the target was added back to the final measured fragment energy in order to center the velocity difference distributions at $v_n - v_f \sim 0$.

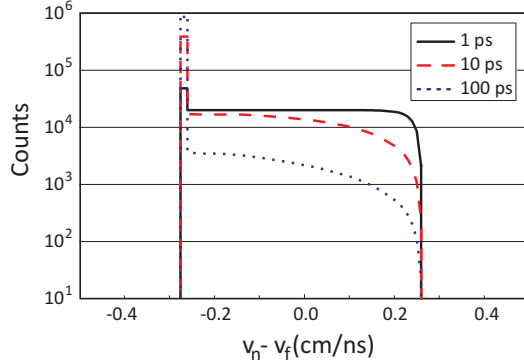


Figure 4: Same as figure 2 assuming that the production can occur anywhere in the target, i.e. the curves from figure 2 were folded with the spread to the energy loss in the target shown by the red/dotted line (700 mg/cm^2) from figure 3.

108 The various effects contributing to the measured distributions are demon-
 109 strated in figures 2-5. Figure 2 shows the calculated velocity difference assuming
 110 that ^{16}B is produced at the beginning of the target. Distributions for half-lives
 111 of 1 ps (black/solid line), 10 ps (red/dotted line), and 100 ps (blue/dashed line)
 112 are shown for a 700 mg/cm^2 thick ^9Be target and an incoming ^{17}C beam en-
 113 ergy of 80 MeV/u . For the calculation of the velocity difference the energy loss
 114 through the full target was added back to the final fragment energy. The expo-
 115 nential decrease of the velocity difference translates directly to the half life. The
 116 beam energy corresponds to a velocity of 11.7 cm/ns and with a target thick-
 117 ness of 0.38 cm , the traversal time through the target is $\sim 32 \text{ ps}$. The decay
 118 rate for a half-life of 10 ps drops by about an order of magnitude during this
 119 time, consistent with the decrease shown by the red/dotted line in the figure.
 120 The sharp increase at the left edge of the distributions is due to the integral of
 121 decays outside of the target which is larger for the longer half-lives.

122 More realistic calculations have to take into account that the reaction can
 123 take place anywhere in the target. Because the exact interaction point is un-
 124 known, the velocity difference broadens due to the varying energy losses by the
 125 fragments in the target. This effect is shown in figure 3 for target thicknesses of

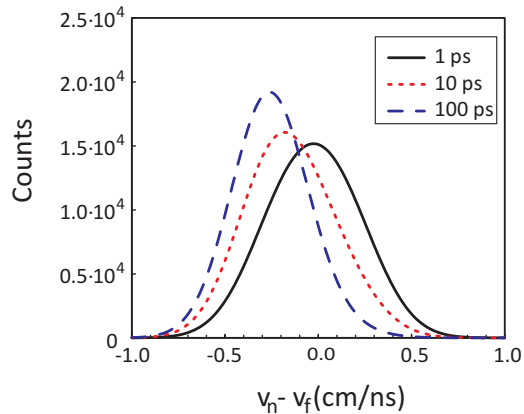


Figure 5: Same as figure 4 folded with the resolution of the velocity measurements.

126 200 mg/cm² (black/solid line), 700 mg/cm² (red/dotted line), and 1500 mg/cm²
 127 (blue/dashed line). The beam energy was 80 MeV/u and it was assumed that
 128 the subsequent decay occurs at the same time/place as the reaction ($t_{1/2} =$
 129 0 ps). In order to center the distributions at $v_n - v_f = 0$, only the energy loss
 130 through half the target thickness was added back to the final fragment energy.

131 The combined effect of finite half-lives and uniform distribution of the re-
 132 action within the target is shown in figure 4 for the same three half-lives and
 133 conditions as in figure 2. Finally, the results of the simulations have to be folded
 134 with realistic resolutions of the detectors. The corresponding curves displayed
 135 in figure 5 were calculated with an overall resolution of 0.2 cm/ns which as-
 136 sumed resolutions (FWHM) of 2% and 3% for the neutron and charged particle
 137 detectors, respectively [15]. The distributions for the half-lives shown in the
 138 figure demonstrate the approximate limits of the method. While the velocity
 139 difference distribution for a half-life of 1 ps is essentially centered around zero,
 140 the distribution for a half-life of 100 ps is centered at the edge of the target and
 141 distributions for longer half-lives are very similar.

142 The general sensitivity of the method can be shown by plotting the average
 143 value of the folded velocity difference distributions as a function of half-lives.
 144 Figure 6 shows the dependence on the target thickness for incident beam ener-

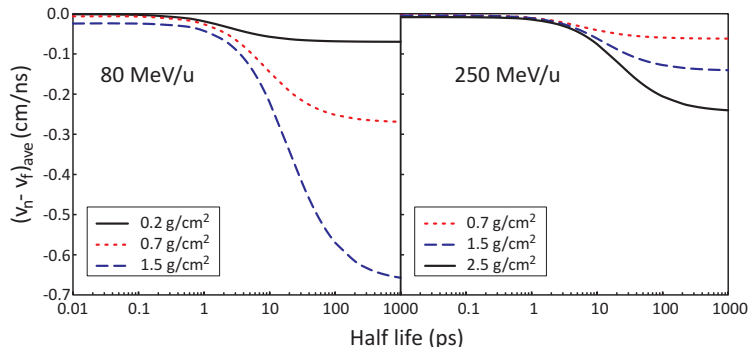


Figure 6: Average value of the velocity difference distributions for the DiT technique as a function of half-life using the reaction $^{17}\text{C}(-p)^{16}\text{B} \rightarrow ^{15}\text{B} + n$ at 80 MeV/u (left) and 250 MeV/u (right) for three different target thicknesses.

145 gies of 80 MeV/u (a) and 250 MeV/u (b). The thicker targets are more sensitive
 146 because the velocity difference depends on the energy loss of the charged frag-
 147 ments in the target. For the same reason, the method is also more effective at
 148 lower energies for the same target thickness.

149 The choice of target thickness for a given energy is limited by the requirement
 150 that the remaining energy after the target has to be sufficiently large to allow
 151 for a clean identification of the fragment and a good energy measurement ($\sim 3\%$
 152 in velocity, see above). Thus at higher energies, thicker targets can be used.
 153 Nevertheless, in order to push the methods to the smallest half-lives it is still
 154 advantageous to use lower beam energies as shown in figure 7. The target
 155 thicknesses of 2700 mg/cm², 700 mg/cm², and 470 mg/cm² for beam energies
 156 of 200 MeV/u (black/solid line), 80 MeV/u (red/dotted line), and 60 MeV/u
 157 (blue/dashed line), respectively, were selected to reach approximately the same
 158 asymptotic value for very long half-lives.

159 In addition to the target thickness and beam energy, the design of an exper-
 160 iment to search for neutron radioactivity has to consider other factors such as
 161 available beam intensity, reaction cross sections and detector resolution. The
 162 most important factor in order to extract a reasonable measurement of a half-

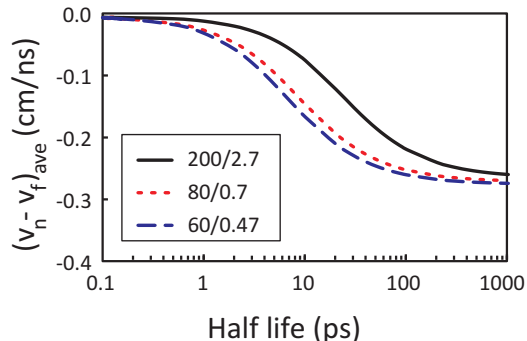


Figure 7: Average value of the velocity difference distributions for the DiT technique as a function of half-life for the reaction $^{17}\text{C}(-p)^{16}\text{B} \rightarrow ^{15}\text{B} + n$ and three different combinations of beam energy and target thicknesses. The first number in the legend corresponds to the beam energy in MeV/u and the second number is the target thickness in g/cm^2 .

163 life will most likely be statistics. At the present time, the beam intensities for
 164 very neutron-rich radioactive beams are still relatively small, although the new
 165 RIBF at RIKEN [22] has achieved some impressive increases. A recent exper-
 166 iment to study the two-neutron decay of ^{26}O with the SAMURAI/NEBULA
 167 setup collected about a factor of 30 more statistics [23] than the published data
 168 from MSU/NSCL [15]. However, the experiment was performed at a higher
 169 incident beam energy (200 MeV/u) with a thicker target ($2 \text{ g}/\text{cm}^2$) and it is not
 170 clear if the increased statistics will be sufficient to make up for the reduction in
 171 sensitivity in the ~ 4 ps range (see figure 7). If the beam energy at RIBF can
 172 be reduced without significant intensity losses SAMURAI/NEBULA is in the
 173 ideal position to improve on the lifetime measurement of ^{26}O .

174 4. Decay in Magnetic Field

175 An alternative method to measure finite lifetimes of neutron emitters pro-
 176 posed by Caesar *et al.* involves the deflection of the fragments in a magnetic
 177 field after the target and measuring the position distribution of the neutrons
 178 [13]. A schematic overview of such an experiment is shown in figure 8. The

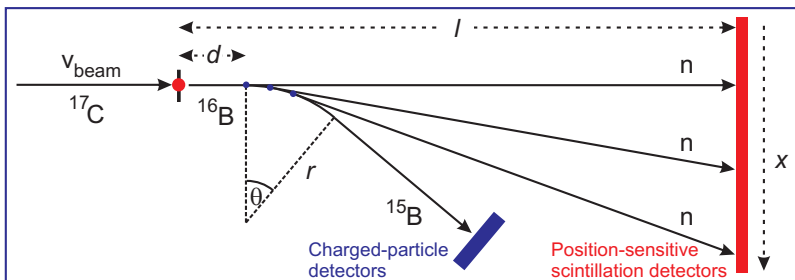


Figure 8: Schematics of the DiMF technique. The incoming ^{17}C beam produces ^{16}B in the target (red dot) which enters a magnet field (bend radius r and deflection angle θ) after a drift distance d . ^{16}B then can decay at different positions along the flight path (blue dots) into ^{15}B and a neutron. The ^{15}B fragments and neutrons are detected and identified in a set of charged-particle detectors and position sensitive scintillation detectors (at a distance l from the target), respectively.

179 reaction [$^{17}\text{C}(-p)^{16}\text{B}$] takes place in the target (red dot) and the subsequent de-
 180 cay ($^{16}\text{B} \rightarrow ^{15}\text{B} + n$) can occur at later times in-flight (blue dots). A deflecting
 181 magnetic field with a bend radius r and a deflecting angle θ bends the charged
 182 particles away from zero degrees after a possible drift distance d into a set of
 183 charged-particle detectors. The neutrons are typically detected with an array of
 184 scintillation detectors [24–27] located near zero degrees at a distance l from the
 185 target. If the lifetime is sufficiently long for ^{16}B to decay within the magnetic
 186 field, the horizontal distribution of the neutrons along the detector is directly
 187 related to the half-life.

188 Figure 9 shows these distributions for six different half-lives. The calcula-
 189 tions were performed at a beam energy of 200 MeV/u and a bend radius of 2 m.
 190 The drift distance was 0 cm and 2-m long neutron detectors were placed at a
 191 distance of 15 m from the target and centered at the beam axis. The results
 192 were folded with a position resolution of 3 cm.

193 Short lifetimes ($\lesssim 10$ ps) result in a shift of the peak of the distributions,
 194 while for longer lifetimes, the exponential decay is directly proportional to an
 195 exponential position decay across the detector which can be expressed by a

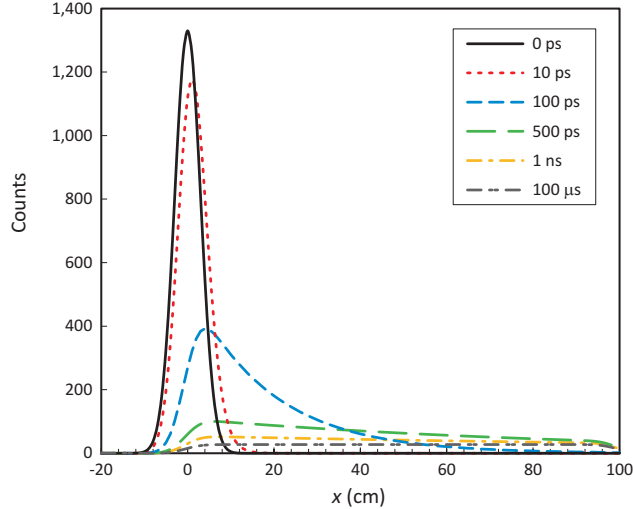


Figure 9: Transverse position distributions for neutrons from the reaction $^{17}\text{C}(-\text{p})^{16}\text{B} \rightarrow ^{15}\text{B} + \text{n}$ at 200 MeV/u for different half-lives. The drift distance, bend radius and neutron detector distances were 0 cm, 200 cm, and 1500 cm, respectively.

196 position decay constant: $\lambda_x = -\ln(\Delta(\text{Counts}))/\Delta x$. The optimum sensitivity
 197 for this arrangement is about 100 ps, where – depending on the statistics of the
 198 experiment – half-lives as short as 10 ps and as long as 1 ns might be measurable.

199 Similar to the DiT technique, in the actual experiment the half-life has to be
 200 extracted from a detailed fit to the whole distribution taking all experimental
 201 parameters into account. However, the sensitivity range of the DiMF method
 202 can be explored by analyzing the average value of the position distributions
 203 (x_{ave}) and the position decay constant λ_x which are shown as a function of
 204 half-lives in the top and bottom panel of figure 10, respectively.

205 The parameters for the three lines shown were selected as approximate repre-
 206 sentations of the experimental setups Sweeper-MoNA at MSU/NSCL (black/solid)
 207 [30, 31], SAMURAI-NEBULA at RIKEN/RIBF (red/dotted) [28], and R³B-
 208 NeuLAND at FAIR (blue/dashed) [27, 29]. The Sweeper-MoNA calculations
 209 were performed for an incoming beam energy of 80 MeV/u, a bend radius of
 210 1 m, and a target to MoNA distance of 8 m. Calculations for the SAMURAI-

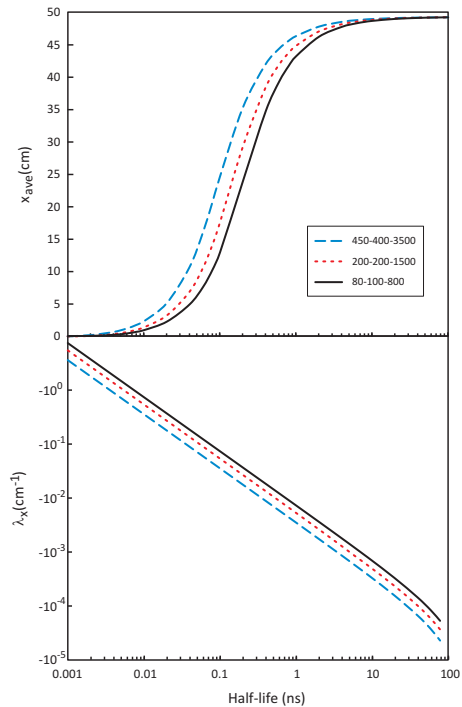


Figure 10: Average position x_{ave} (top) and position decay constant λ_x (bottom) of the transverse position distributions for neutrons from the reaction $^{17}\text{C}(-p)^{16}\text{B} \rightarrow ^{15}\text{B} + n$ as a function of half-lives. The numbers in the legend box correspond to the incoming beam energy in MeV/u, bend radius in cm, and neutron detector distance in cm.

211 NEBULA setup assumed a beam energy of 200 MeV, a bend radius of 2 m and
 212 a neutron time-of-flight distance of 15 m. The corresponding values for R³B-
 213 NeuLAND were 450 MeV/u, 4 m and 35 m. It should be stressed that for all
 214 calculations the target was placed directly in front of the magnet with a drift
 215 distance of 0 m.

216 The most important parameter to reach sensitivities for short lifetimes is the
 217 beam energy. However, even at the highest beam energies it will be difficult to
 218 reach sensitivities below about 10 ps. The bend radius and the neutron time-
 219 of-flight distance are directly proportional, i.e. for a given beam energy a bend
 220 radius of 1 m and detector distance of 5 m is equivalent to a radius of 3 m and

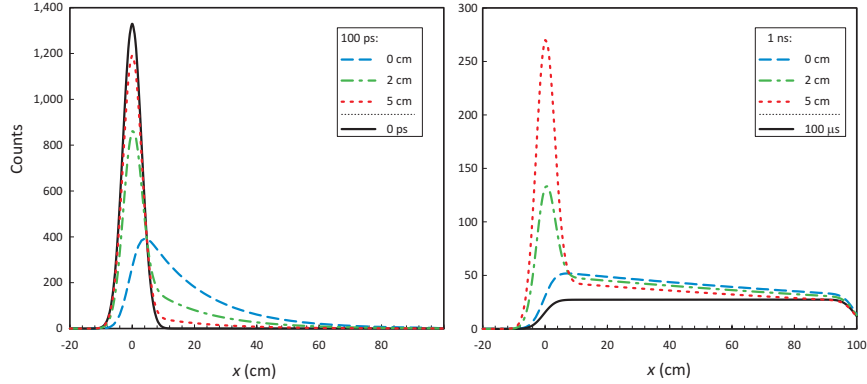


Figure 11: Transverse position distributions for neutrons from the reaction $^{17}\text{C}(-\text{p})^{16}\text{B} \rightarrow ^{15}\text{B} + \text{n}$ at 200 MeV/u and half-lives of 100 ps (left) and 1 ns (right). Distributions for drift distances of 0 cm (blue/dashed line) 2 cm (green/dot-dashed line) and 5 cm (red/dotted line) are shown. For reference, the distributions for half-lives of 0 ps and 100 μs for 0 cm drift distance (black/solid line) are included in the left and right panel, respectively. The calculations were performed for the same number of reactions. Note the difference in the vertical scales.

221 a distance of 15 m.

222 While x_{ave} is more sensitive to shorter lifetimes, λ_x is more relevant for longer
 223 lifetimes. The sensitivity limits can be estimated by comparing the red curves in
 224 figure 10 with the approximate parameters for the SAMURAI-NEBULA setup
 225 with the distributions of figure 9 which were calculated with the same parame-
 226 ters. The lower limit for extracting a half-life of ~ 10 ps is determined from the
 227 lower limit of measuring the shift of x_{ave} at about 2 cm, while the upper limit
 228 of ~ 1 ns is due the limit of measuring λ_x at about -0.01 cm^{-1} .

229 The importance of placing the target directly in front of the deflecting mag-
 230 net is demonstrated in figure 11. Especially for the shorter lifetimes, it will be
 231 critical to locate the target as close as possible to the magnet. As shown in
 232 the left panel of the figure, for a half-life of 100 ps a drift distance as small as
 233 2 cm already moves the peak of the distribution to the center with only a tail
 234 extending to larger distances. For longer lifetimes the drift distance is not as

235 critical. Although a certain fraction of the events will accumulate in a peak at
236 the center, the position decay constant of the distribution remains the same and
237 the overall intensity of the tail is not significantly reduced (see the right panel
238 of the figure).

239 **5. Conclusions**

240 Two methods to search for neutron radioactivity were discussed. In the
241 first method the velocity difference of the neutrons and the charged fragments
242 is measured. This method is sensitive to decays that occur within the target
243 (DiT) and depends on the energy loss of the charged fragment in the target.
244 The second method is sensitive to decays in-flight after the target by relying on
245 the deflection of the charged fragment in a magnetic field (DiMF) which will
246 then translate into the horizontal distribution of the neutrons. In order to be
247 sensitive to the shortest lifetimes, the DiT method is better at low beam energies
248 while the DiMF method is more sensitive at high beam energies. Within the
249 range of presently available beam energies and experimental setups the DiT
250 method is more sensitive to half-lives in the 1–100 ps range, while the DiMF
251 method is sensitive to half-lives between ~ 10 ps and ~ 1 ns.

252 **Acknowledgments**

253 This work was supported by the National Science Foundation under grant
254 PHY-11-02511. We would like to thank P. DeYoung, J. E. Finck, R. Haring-
255 Kaye, and S. Stephenson for valuable comments and careful reading of the
256 manuscript.

257 **References**

- 258 [1] M. Pfützner, Phys. Scr. **T152**, 014014 (2013)
259 [2] R. A. Kryger *et al.*, Phys. Rev. C **53**, 1971 (1996)

- 260 [3] L. V. Grigorenko, I. G. Mukha, C. Scheidenberger, and M. V. Zhukov,
261 Phys. Rev. C **84**, 021303(R) (2011)
- 262 [4] T. Baumann, A. Spyrou, M. Thoennessen, Rep. Prog. Phys. **75**, 036301
263 (2012)
- 264 [5] M. Thoennessen, Rep. Prog. Phys. **67**, 1187 (2004)
- 265 [6] S. N. Liddick *et al.*, Phys. Rev. Lett. **97**, 082501 (2006)
- 266 [7] R. Grzywacz *et al.*, Nucl. Instrum. Meth. B **261**, 1103 (2007)
- 267 [8] C. R. Bingham *et al.*, Nucl. Instrum. Meth. B **241**, 185 (2005)
- 268 [9] R. Grzywacz *et al.*, Eur. Phys. J. A **25**, s01, 145 (2005)
- 269 [10] K. P. Rykaczewski *et al.*, AIP Conf. Proc. **764**, 223 (2005)
- 270 [11] I. Mukha *et al.*, Phys. Rev. Lett. **99**, 182501 (2007)
- 271 [12] P. Voss *et al.*, subm. to Phys. Rev. C, P. Voss, *Recoil distance method*
272 *lifetime measurements via gamma-ray and charged-particle spectroscopy at*
273 *NSCL*, Ph. D. thesis, Michigan State University, unpublished (2011),
274 http://www.nsl.msu.edu/ourlab/publications/download/Voss2011_278.pdf
- 275 [13] C. Caesar *et al.*, arXiv:1209.0156v2
- 276 [14] E. Lunderberg *et al.*, Phys. Rev. Lett. **108**, 142503 (2012)
- 277 [15] Z. Kohley *et al.*, Phys. Rev. Lett. **110**, 152501 (2013)
- 278 [16] J. D. Bowman, A. M. Poskanzer, R. G. Korteling, and G. W. Butler, Phys.
279 Rev. C **9**, 836 (1974)
- 280 [17] M. Langevin *et al.*, Phys. Lett. B **150**, 71 (1985)
- 281 [18] R. Kalpakchieva *et al.*, Eur. Phys. J. A **7**, 451 (2000)
- 282 [19] H. G. Bohlen *et al.*, Nucl. Phys. A **583**, 775c (1995)

- 283 [20] J.-L. Lecouey *et al.*, Phys. Lett. B **672**, 6 (2009)
- 284 [21] A. Spyrou *et al.*, Phys. Lett. B **683**, 129 (2010)
- 285 [22] Y. Yano, Nucl. Instrum. Meth. B **261**, 1009 (2007)
- 286 [23] Y. Kondo *et al.*, *4th International Conference on Collective Motion in Nu-*
287 *clei under Extreme Conditions COMEX4*, October 22–26, 2012, Shonan
288 Village Center, Kanagawa, Japan; T. Nakamura, private communication
- 289 [24] T. Blaich *et al.*, Nucl. Instrum. Meth. A **314**, 136 (1992)
- 290 [25] T. Baumann *et al.*, Nucl. Instrum. Meth. A **543**, 517 (2005)
- 291 [26] K. Yoneda *et al.*, RIKEN Accel. Prog. Rep. **43**, 178 (2010)
- 292 [27] *Technical Report for the Design, Construction and Commissioning of*
293 *NeuLAND: The High-Resolution Neutron Time-of-Flight Spectrometer for*
294 *R³B*,
295 [http://www.fair-center.eu/fileadmin/fair/experiments/NUSTAR/Pdf/TDRs/NeuLAND-](http://www.fair-center.eu/fileadmin/fair/experiments/NUSTAR/Pdf/TDRs/NeuLAND-TDR-Web.pdf)
296 [TDR-Web.pdf](http://www.fair-center.eu/fileadmin/fair/experiments/NUSTAR/Pdf/TDRs/NeuLAND-TDR-Web.pdf)
- 297 [28] *Large-Acceptance Multi-Particle Spectrometer SAMURAI*, Presentation at
298 RIBF TAC05, RIKEN, Japan, 17–19 November 2005
299 http://ribf.riken.go.jp/RIBF-TAC05/10_SAMURAI.pdf
- 300 [29] B. Gastineau *et al.*, IEEE Trans. Appl. Supercond. **18**, 407 (2008)
- 301 [30] M. D. Bird *et al.*, IEEE Trans. Appl. Supercond. **15**, 1252 (2005)
- 302 [31] Z. Kohley *et al.*, Nucl. Instrum. Meth. A **682**, 59 (2012)